Effect of cation arrangement on the electronic structures of the perovskite solid solutions $(SrTiO_3)_{1-x}(LaCrO_3)_x$ from first principles

Hungru Chen[1] and Naoto Umezawa[1,2,3,*]

[1]*Environmental Remediation Materials Unit, National Institute for Materials Sciences, Ibaraki 305-0044, Japan*

[2]*PRESTO, Japan Science and Technology Agency (JST), 4-1-8 Honcho Kawaguchi, Saitama 332-0012, Japan*

[3]*TU-NIMS Joint Research Center, School of Materials Science and Engineering, Tianjin University,*

92 Weijin Road, Nankai District, Tianjin, P.R. China

The electronic structures of $[SrTiO_3]_{1-x}[LaCrO_3]_x$ perovskite solid solutions are studied using hybrid density functional calculations to investigate their potential photocatalytic activity. The introduction of Cr^{3+} into $SrTiO_3$ not only creates occupied states inside the band gap but can adversely narrow the conduction band. However, if Cr^{3+} and Ti^{4+} ions are segregated in alternating [001] layers, the conduction band remains highly dispersive. This suggests that the electronic structure can be tuned by controlling the cation arrangement. We predict that $[SrTiO_3]_{0.5}[LaCrO_3]_{0.5}$ with alternating TiO_2 and CrO_2 layered along the [001] direction, which has not been experimentally realized yet, will exhibit strong absorption of visible light response and excellent electronic transport properties.

PACS number(s): 82.45.Jn, 71.20.−b

I. INTRODUCTION

Strontium titanate $SrTiO_3$ (STO) is a prototypical perovskite oxide in which Sr occupies the 12-fold cuboctahedral site (*A*-site) and Ti occupies the sixfold octahedral site (*B*-site). STO has attracted much attention due to association with a variety of fascinating physical properties such as superconductivity [1], ferroelectricity [2], and the formation of a two-dimensional electron gas on its surface, as well as at the interface between STO and $LaAlO_3$ [3,4]. STO is also a promising material for the generation of hydrogen fuel by photoelectrolysis. A photoelectrochemical cell with a single crystal STO anode can split water even without applying an additional bias voltage [5]. The powder form of STO can also decompose water under suitable conditions [6]. However, the large band gap of between 3.2 and 3.4 eV based on optical measurements [7–9] limits the solar energy conversion efficiency of STO. This is because the electron-hole pairs that are necessary to initiate photocatalytic reactions can only be generated by the absorption of light in the ultraviolet range, which comprises a small fraction of the solar spectrum.

Doping with transition metals has been a common approach in attempts to sensitize STO to visible light. Various studies have found that small concentrations of Cr^{3+} give rise to an optimal visible light response [10–13]. Photocurrent measurements [11,14,15] have shown that this is associated with an absorption peak at ~ 450 nm, attributed to a $Cr \rightarrow Ti$ charge transfer transition. Subsequent studies on powder samples of Cr^{3+}-doped STO have confirmed that photocatalytic activity takes place under visible light [16–19]. The charge imbalance caused by substituting Cr^{3+} for Ti^{4+} can be compensated by a simultaneous *A*-site substitution, for example replacing Sr^{2+} with La^{3+}. This avoids the formation of oxygen vacancies, which are commonly believed to act as charge carrier recombination centers.

Despite the sensitization ability of Cr^{3+}, the photocurrent activity of Cr^{3+}-doped STO is significantly lowered, even when the energy is sufficient for band gap excitation [14]. Furthermore, a study on Cr^{3+}-doped colloidal TiO_2 particles showed that whereas a low concentration of Cr^{3+} induces visible light response, the activity decreases drastically with increasing Cr^{3+} content [20]. This adverse effect has been explained by a lowering of the diffusion lengths of minority carriers, i.e., photogenerated holes, because Cr^{3+} cations act as hole traps [10]. However, in STO only, photogenerated electrons contribute to the photocurrent; the mobility of photogenerated holes is rather low probably due to immediate trapping after generation [21–23]. Therefore, hole trapping by Cr^{3+} should not have an adverse effect on the photocurrent.

Prompted by the sensitization ability of the Cr^{3+} ion in STO and by the fact that STO and $LaCrO_3$ (LCO) form a complete solid solution series $STO_{1-x}LCO_x$ with $0 \leqslant x \leqslant 1$ [24–26], we calculated the electronic structures of $STO_{1-x}LCO_x$ solid solutions using density functional theory to clarify the effect of Cr^{3+} and to assess the potential of these solid solutions as efficient visible-light-driven photocatalysts. Our computational results show that the electronic structure depends significantly on the *B*-site cation arrangement. That is, the dispersion of the conduction band is significantly weakened when the planar Ti-O-Ti network is disrupted by the presence of Cr^{3+}. This finding gives an alternative explanation to the lowered quantum efficiency of STO upon Cr^{3+} doping and allows a strategy to be proposed for the design of novel perovskite photocatalysts with highly dispersive conduction bands and the ability to strongly absorb visible light. Recently, perovskite [001] heterostructures have also been predicted to have a high solar energy conversion efficiency [27].

II. METHODOLOGY

All calculations were based on density functional theory, utilizing the range- separated screened hybrid functional Heyd-Scuseria-Ernzerhof (HSE) [28], which mixes 25%

*Corresponding author: umezawa.naoto@nims.go.jp

Hartree-Fock exchange with 75% of the generalized gradient approximation (GGA) Perdew-Burke-Ernzerhof [29] (PBE) functional. The inclusion of Hartree-Fock exchange in the HSE functional is known to greatly improve the description of transition metal oxides over local density approximation (LDA) and GGA functionals. The experimental lattice constants and band gaps of STO and LCO are well reproduced by previous HSE calculations [30,31], and values obtained in this study differ from those by less than 1%. Interactions between the core and valence electrons were treated by the projector augmented wave approach [32]. The cutoff energy for plane waves was set at 500 eV. For all cells calculated, the k-point spacing was smaller than 0.03 Å^{-1} in the Brillouin zone. Structural optimization of lattice vectors and atomic positions was performed on all of the cells until the forces converged to less than 0.01 eV-Å^{-1} per ion. All calculations were carried out using the Vienna *Ab initio* Simulation Package (VASP) [33].

The STO$_{1-x}$LCO$_x$ solid solutions were modeled by using perovskite supercells in which Sr and La occupy the A-site and Ti and Cr occupy the B-site [34]. The two end members of the solid solution series, STO and LCO, adopt primitive cubic and orthorhombic perovskite structures at room temperature, with space group symmetries *Pm*-3*m* (one formula unit per cell) and *Pnma* (four formula units per cell), respectively [35,36]. The structure of the STO$_{1-x}$LCO$_x$ solution has been observed to transform from cubic to orthorhombic as the concentration x increases [24–26]. Accordingly, the STO$_{1-x}$LCO$_x$ solid solutions at $x = 0.125, 0.25$, and 0.5 were simulated using not only supercells based on the cubic unit cell but also based on the orthorhombic unit cell, which allows the tilting of TiO$_6$ octahedra. In all calculated cells, unless described specifically, each of the substituted La–Cr pairs is located as nearest neighbors, and same cation arrangements are adopted in both A-site and B-site cation sublattices.

III. RESULTS AND DISCUSSION

A. Pristine SrTiO$_3$

We first discuss the electronic structure of cubic STO. From the calculated electronic band structure shown in Fig. 1(a), STO is a band insulator with a band gap separating the O 2p states that dominate the valence band from the Ti 3d states
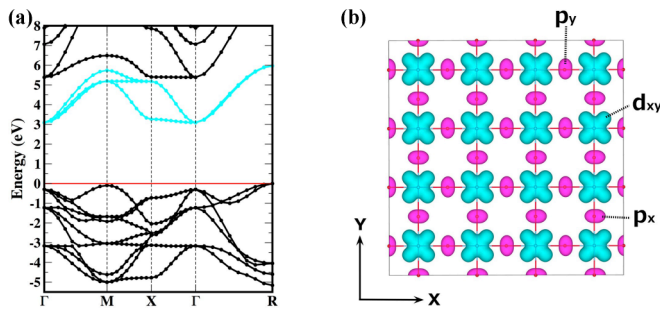
that dominate the conduction band. The calculated band gap is ~3.3 eV, in good agreement with optical measurements [8,9]. The five Ti d states are split by the octahedral crystal field into three lower t_{2g} (d_{xy}, d_{yz}, d_{xz}) bands and two upper e_g ($d_{x^2-y^2}$, d_{z^2}) bands. The width/dispersion of the t_{2g} bands is relevant to the effective mass, and hence the mobility of the electrons, and is ~2.8 eV from our calculations. Efficient photocatalysis requires that photoexcited electron reach the surface of the material rapidly before recombination. The high mobility of photogenerated electrons in STO [21,22] certainly has an important contribution to its high photocatalytic activity.

In the perovskite structure, the distance between neighboring B-site Ti cations is large; hence, direct t_{2g} orbital overlap is negligible. The width of the t_{2g} bands results predominantly from an interaction mediated by oxygen; the t_{2g} orbitals on neighboring Ti cations overlap with the intermediate oxygen 2p orbitals [37,38], referred to as a $pd\pi$ interaction, as illustrated in Fig. 1(b). Due to the planar character of the $pd\pi$ interaction, the t_{2g} conduction bands also have a two-dimensional character [39], despite the cubic crystal symmetry of STO. This can be understood by looking at the band structure in Fig. 1(a). Along the cubic crystal axis ($\Gamma \rightarrow X$), one of the three t_{2g} bands is nearly flat, whereas the other two are degenerate and highly dispersive. This implies that electrons in one of the three bands have high effective mass along one crystal axis but low effective mass along the other two axes. For example, the width/dispersion of the d_{xy} state shown in Fig. 1(b) arises from the $pd\pi$ interaction in the xy plane. Here the effective mass is low in the xy plane but high along the z direction. Similarly, the widths/dispersions of the d_{yz} and d_{xz} bands result from $pd\pi$ interactions in the yz and xz planes, respectively.

B. STO$_{1-x}$LCO$_x$ solid solutions

In a perovskite supecell representing the STO$_{1-x}$LCO$_x$ solid solution at a given concentration x, two different cations, Sr and La, are present at the A-site, and two different cations, Ti and Cr, are present at the B-site. Hence, there are many possible A-site and B-site cation arrangements as well as their combinations. Besides, the cell can be constructed either from the cubic STO primitive cell without octahedral tilting or from the orthorhombic LCO primitive cell with octahedral tilting. First we would like to exclude the effect of A-site cation arrangement and octahedral tilting on the electronic structure; therefore, our later discussion can be confined only to the effect of the B-site cation arrangement. Here we demonstrate, by using the case of STO$_{0.5}$LCO$_{0.5}$, the insignificance of A-site cation arrangement and octahedral tilting.

Figure 2 shows the density of states of STO$_{0.5}$LCO$_{0.5}$ calculated from three different structural models with the same B-site cation arrangement. The top structure differs from the middle one only in the A-site cation arrangement. As seen from the density of states, there is no noticeable difference in their electronic structures from rearranging the A-site cations. It has also been confirmed that all the other possible A-site cation arrangements yield essentially the same electronic structures in terms of the shape and the position of valence band and conduction band edges in density of states. Next we will show the effect of octahedral tilting on
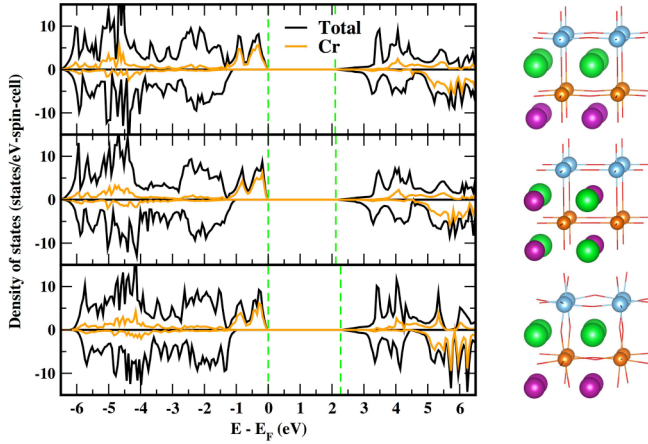

FIG. 1. (Color online) (a) Calculated band structure of cubic SrTiO$_3$. The top of the valence band is positioned at 0 eV. The three t_{2g} conduction bands are highlighted in cyan. (b) Illustration of $pd\pi$ interactions in the xy plane. Blue and pink shading denote the Ti d_{xy} and O p orbitals, respectively.

FIG. 2. (Color online) Density of states of $STO_{0.5}LCO_{0.5}$ with different A-site cation orderings and their structural models. The green dashed lines indicate the edges of the occupied and unoccupied states. The blue, orange, green, and purple spheres denote Ti^{4+}, Cr^{3+}, Sr^{2+}, and La^{3+} cations, respectively. Oxygens are omitted for clarity. Ti-O and Cr-O bonds are shown as sticks.

the electronic structure. As seen in Fig. 2, the bottom structure differs from the top structure in its octahedral tilting. Such tilting makes the Ti-O-Ti bond length deviate from 180° and results in the reduction of the Ti t_{2g} bandwidth [40] and a concomitant 0.15 eV upshift of the conduction band minimum (CBM). This effect is relatively small compared to the effect of rearranging the B-site cations, which can give rise to a considerable 1.9-eV upshift of the CBM, as will be discussed below. In cells with lower LCO concentrations considered in this work, $x = 0.125$ and 0.25, the Ti-O-Ti bonds are less distorted than those in the $x = 0.5$ cell; therefore, the effect of octahedral tilting becomes even smaller.

We have shown above that the A-site cation arrangement and octahedral tilting have no noticeable effect on the electronic structure. In the discussion that follows, only the results obtained from the supercells based on the cubic unit cell are presented, and the A-site cation arrangement will not be discussed further. To see how the electronic structure changes as the concentration x increases, first a simple cation arrangement in $STO_{1-x}LCO_x$ solid solutions is considered in which all Cr^{3+} ($t_{2g}{}^3 e_g{}^0$) ions are confined to one layer. Figure 3 shows the structural models and their corresponding densities of states for $x = 0$, 0.037, 0.125, 0.25, and 0.5. When a small concentration of LCO is incorporated into STO, as in the case of $x = 0.037$, occupied Cr^{3+} t_{2g} states appear in the band gap above the valence band maximum (VBM) of STO. Therefore, charge transfer transition from Cr to Ti is expected under photoirradiation with an excitation energy smaller than the original band gap O $2p$ to Ti $3d$ transition and is in agreement with the 450-nm absorption peak observed experimentally for STO doped with a small concentration of Cr^{3+}. As the concentration of LCO increases, the density of occupied Cr^{3+} t_{2g} states inside the band gap also increases, whereas the position of the Ti CBM relative to the O $2p$ VBM is not changed. Intuitively, the increasing concentration of LCO should thus be accompanied by a higher rate of Cr → Ti charge transfer transition and enhance the visible
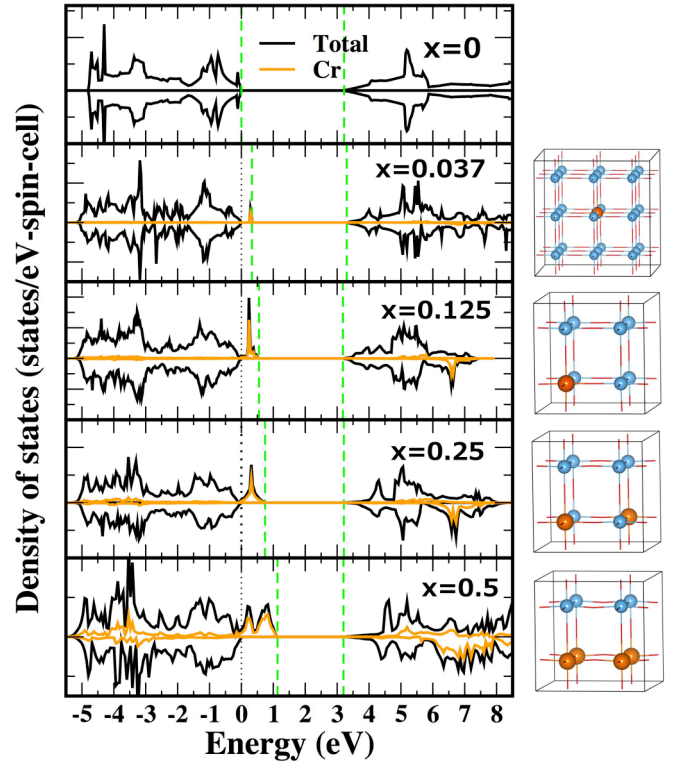

FIG. 3. (Color online) Calculated density of states of $STO_{1-x}LCO_x$ solid solutions (left) and structural models (right) for $x = 0$, 0.037, 0.125, 0.25, and 0.5. The green dashed lines indicate the edges of the occupied and unoccupied states. The tops of the oxygen $2p$ states at each concentration are aligned at 0 eV. The blue and orange spheres in the structural models denote Ti^{4+} and Cr^{3+} cations, respectively. Sr^{2+}, La^{3+}, and O^{2-} ions are omitted for clarity.

light photocatalytic activity. However, this is inconsistent with the experimentally observed adverse effect of increasing the concentration of Cr^{3+}. One possible problem is that our structural models are highly ordered; thus, it is unclear whether the electronic structures obtained from them are valid for real $STO_{1-x}LCO_x$ solid solutions in which the cations are disordered [25,26].

In order to investigate the effect of the B-site cation arrangement, alternative structural models were considered. Surprisingly, the B-site cation arrangement significantly influences the electronic structure. The upper panel of Fig. 4 shows two different B-site cation arrangements for $x = 0.25$, labeled $STO_{0.75}LCO_{0.25}$ (A) and $STO_{0.75}LCO_{0.25}$ (B), and their electronic band structures. In the band structure of $STO_{0.75}LCO_{0.25}$ (A), the spin-up and spin-down t_{2g} conduction bands both range from energies of 3.2 to 6 eV with widths of 2.8 eV, similar to pristine STO. However, if the B-site cations are rearranged to form the $STO_{0.75}LCO_{0.25}$ (B) configuration, the t_{2g} bandwidth in the spin-up channel is decreased to 1.5 eV with a concomitant upward shift of the CBM. Analogous changes are observed in the spin-down channel, but to a lesser extent. The dependence of the electronic structure on the B-site cation arrangement is even more striking in the case of $x = 0.5$. The lower panel of Fig. 4 shows two structural models $x = 0.5$, labeled $STO_{0.5}LCO_{0.5}$ (A) and $STO_{0.5}LCO_{0.5}$ (B), together with their corresponding electronic band structures.

STO$_{0.75}$LCO$_{0.25}$ (A)

STO$_{0.75}$LCO$_{0.25}$ (B)
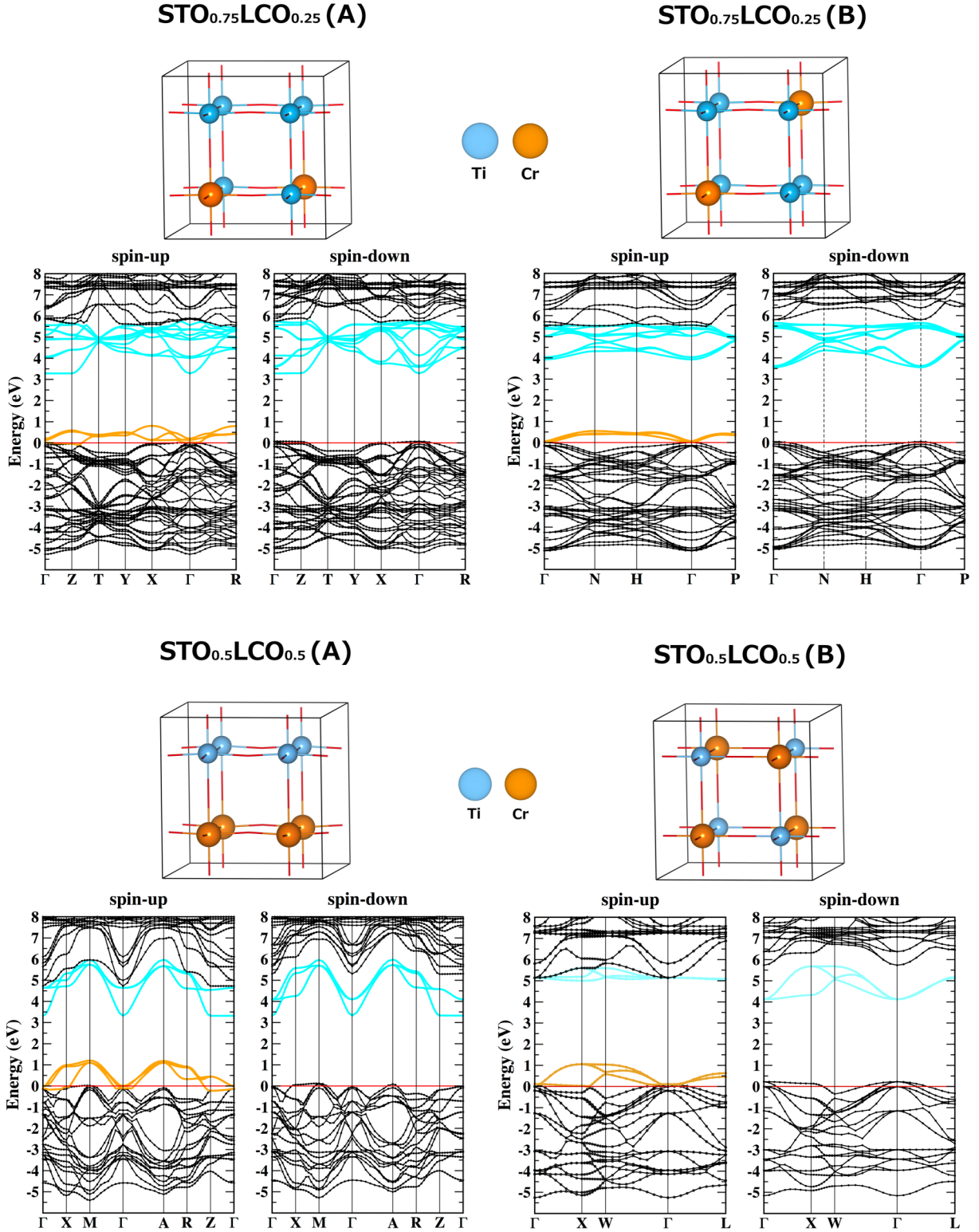
STO$_{0.5}$LCO$_{0.5}$ (A)

STO$_{0.5}$LCO$_{0.5}$ (B)

FIG. 4. (Color online) Structural models for different cation arrangements in STO$_{0.75}$LCO$_{0.25}$ (upper panel) and STO$_{0.5}$LCO$_{0.5}$ (lower panel) with their calculated band structures. In the structural models, Sr^{2+}, La^{3+}, and O^{2-} ions are omitted for clarity. In the band structure plots, orange lines denote the occupied Cr^{3+} states and the cyan curves denote Ti t_{2g} states. The tops of the oxygen 2p states are aligned at 0 eV.

For STO$_{0.5}$LCO$_{0.5}$ (A), the t_{2g} conduction bands remain highly dispersive with a bandwidth 2.8 eV, as in pristine STO. In contrast, the spin-up t_{2g} bands for STO$_{0.5}$LCO$_{0.5}$ (B) exhibit almost no dispersion, and the CBM is located at 5.1 eV higher

than the oxygen 2p VBM. Furthermore, the width of the spin-down t_{2g} conduction band is narrowed to 1.8 eV.

The reduction of the Ti t_{2g} bandwidth in STO$_{0.75}$LCO$_{0.25}$ (B) and STO$_{0.5}$LCO$_{0.5}$ (B) implies that the presence of
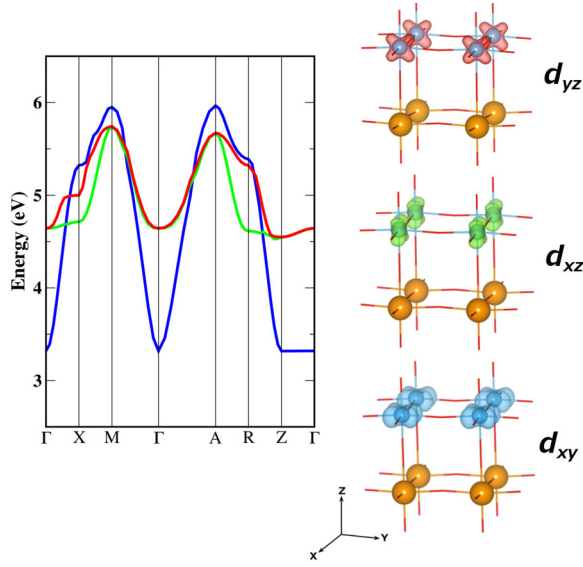
FIG. 5. (Color online) Enlarged view of the three spin-up Ti t_{2g} bands in $STO_{0.5}LCO_{0.5}$ (A) (left) and their spatial character at the Γ point (right). The blue, green, and red curves in the band structure plot and the blue, green, and red shaded isosurfaces denote the d_{xy}, d_{xz}, and d_{yz} states, respectively.

FIG. 6. (Color online) A schematic illustration of the electron hopping process.

Cr^{3+} ions in these structures interrupts the extended $pd\pi$ interactions, which determine this bandwidth, as discussed above. However, this raises the question of why the conduction bandwidth in $STO_{0.75}LCO_{0.25}$ (A) and $STO_{0.5}LCO_{0.5}$ (A) remains intact even in the presence of Cr^{3+}. This issue can be understood by a detailed examination of the band structure of $STO_{0.5}LCO_{0.5}$ (A). Figure 5 shows the dispersion of the three t_{2g} bands in $STO_{0.5}LCO_{0.5}$ (A) and their charge densities at the Γ point. At first glance, the overall width of the t_{2g} bands is not diminished by the presence of Cr^{3+}. However, if the three bands are examined separately, only the d_{xy} band remains highly dispersive, whereas the d_{yz} and d_{xz} bands are significantly narrowed, and their minima at the Γ point are shifted upward to a position 4.7 eV higher than the oxygen $2p$ VBM. This is due to the absence of Cr^{3+} in the upper xy plane of the structure, allowing undisturbed $pd\pi$ interactions. In contrast, the presence of Cr^{3+} in the yz and xz planes interrupts the $pd\pi$ interactions in these directions causing a reduction of the d_{yz} and d_{xz} bandwidths.

The physical mechanism for the reduction of the t_{2g} bandwidth due to the presence of Cr^{3+} ions is demonstrated in the electron hopping process shown in Fig. 6. The t_{2g} orbitals of Ti^{4+} ($t_{2g}{}^0 e_g{}^0$) are all empty; therefore, a t_{2g} electron can hop between Ti^{4+} sites freely. However, the three t_{2g} orbitals of Cr^{3+} ($t_{2g}{}^3 e_g{}^0$) are all occupied by spin-up electrons. Consequently the hopping of a spin-up t_{2g} electron onto the Cr^{3+} site is forbidden by the Pauli principle. This explains the difference in bandwidth reduction between spin-up and spin-down electrons in Fig. 4. Besides, while a spin-down electron is allowed to hop onto the Cr^{3+} site, it would experience an onsite Coulomb repulsion, which is absent or less significant at the Ti^{4+} site, because of the presence of three electrons that already occupy the Cr^{3+} site. Therefore,
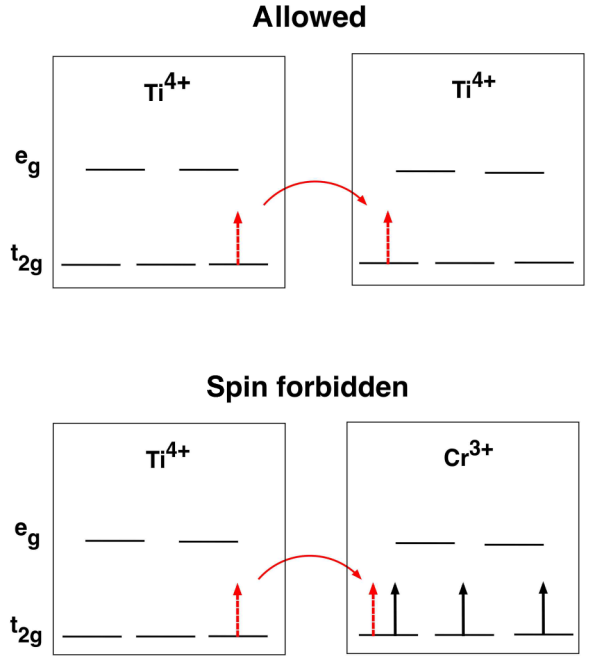
the reduction of spin-down t_{2g} bandwidth also occurs, although to a lesser extent compared to spin-up bands.

IV. CONCLUSIONS

In summary, we have shown that the presence of Cr^{3+} in $STO_{1-x}LCO_x$ solid solutions not only creates occupied states in the band gap but can also alter the character of the conduction band. Because the width of the Ti t_{2g} conduction bands is determined by the Ti-O $pd\pi$ interactions, the presence of Cr^{3+} on the B-site disrupts these interactions and results in a reduction of the bandwidth. In addition, the two-dimensional character of the t_{2g} conduction bands leads to a strong dependence of the electronic structure on the B-site cation arrangement. A random distribution of Cr^{3+} on the B-site, as previously reported for $STO_{1-x}LCO_x$ solid solutions, disrupts the Ti-O $pd\pi$ interactions in all three xy, yz, and xz planes. Consequently, as the concentration of Cr^{3+} increases, the bandwidth of all three Ti t_{2g} states, d_{xy}, d_{yz}, and d_{xz}, becomes narrower, and the CBM is shifted upward. This gives rise to two detrimental effects on the photocatalytic activity. First, the narrowing of the t_{2g} bandwidth corresponds to an increase of the electron effective mass. This amplifies the rate of electron-hole recombination and hinders the photocatalytic activities. Second, the upward shift of the CBM results in increased energies for both the O $2p \rightarrow$ Ti $3d$ and $Cr \rightarrow$ Ti transitions. Consequently, an electron-hole pair can only be generated by the absorption of light with shorter wavelengths, which lowers the solar energy conversion efficiency.

Nevertheless, we have also shown that if Cr and Ti can be segregated into alternating [001] layers, one of the t_{2g} states remains highly dispersive. This implies that the effective mass for that t_{2g} state is low (high mobility) and that the position of the CBM will not be affected even at high Cr^{3+} concentration,

as in the case of $STO_{0.5}LCO_{0.5}$ (A). Therefore, we predict that $STO_{0.5}LCO_{0.5}$ grown with TiO_2 and CrO_2 layers alternating along the [001] direction will be an excellent material for solar energy conversion in which the CrO_2 layers are responsible for visible light absorption and the TiO_2 layers are responsible for electron migration. Possible experimental realizations of such an alternating layered structure are discussed in the Appendix. Our findings suggest a strategy for the design of visible-light-sensitive perovskite oxide materials with high electron mobility by utilizing the two-dimensional character of the t_{2g} conduction bands.

APPENDIX

Here we remark on the possibilities of realizing the proposed layered structure. The previously reported $STO_{0.5}LCO_{0.5}$ solid solutions synthesized by conventional high-temperature solid state reactions are cation disordered [25,26], which indicates that the [001] layered ordering is not the most thermodynamically stable or not stable enough to retain at high temperature. Nonetheless, recent development on advanced material synthesis methods has enabled us to overcome the thermodynamic barrier. Many artificial oxide structures have been experimentally fabricated [41] and theoretically studied [42]. An alternating layer of a LCO-LaFeO$_3$ superlattice with [100] stacking direction that is very similar to our proposed structure has been synthesized using a multitarget pulsed laser deposition technique [43]. Such thin film can be grown on a substrate with a step-terrace structure so that the side of the thin film will be largely exposed for charge transfer out of the material [44]. Apart from epitaxial thin-film growth techniques, low-temperature soft chemistry routes are also capable of preparing nonthermodynamically stable (metastable) phases that are not accessible by conventional solid state reactions. For example, various oxide nanosheets with atomic thickness have been synthesized, and they can be arbitrarily stacked to form superlatticelike structures [45,46]. In addition, very recently a perovskite compound Ca_2FeMnO_6 with [100] layered ordering was successfully synthesized by low-temperature oxidation from brownmillerite Ca_2FeMnO_5, which is inherently layered [47]. All above examples suggest that it is possible to synthesize the proposed layered $STO_{0.5}LCO_{0.5}$, a task we are currently working on.

[1] J. F. Schooley, W. R. Hosler, and M. L. Cohen, Phys. Rev. Lett. **12**, 474 (1964).

[2] J. H. Haeni, P. Irvin, W. Chang, R. Uecker, P. Reiche, Y. L. Li, S. Choudhury, W. Tian, M. E. Hawley, B. Craigo, A. K. Tagantsev, X. Q. Pan, S. K. Streiffer, L. Q. Chen, S. W. Kirchoefer, J. Levy, and D. G. Schlom, Nature **430**, 758 (2004).

[3] A. Ohtomo and H. Y. Hwang, Nature **427**, 423 (2004).

[4] A. F. Santander-Syro, O. Copie, T. Kondo, F. Fortuna, S. Pailhès, R. Weht, X. G. Qiu, F. Bertran, A. Nicolaou, A. Taleb-Ibrahimi, P. Le Fèvre, G. Herranz, M. Bibes, N. Reyren, Y. Apertet, P. Lecoeur, A. Barthélémy, and M. J. Rozenberg, Nature **469**, 189 (2011).

[5] J. G. Mavroides, J. A. Kafalas, and D. F. Kolesar, Appl. Phys. Lett. **28**, 241 (1976).

[6] K. Domen, S. Naito, T. Onishi, and K. Tamaru, Chem. Phys. Lett. **92**, 433 (1982).

[7] Y. Yamada and Y. Kanemitsu, Phys. Rev. B **82**, 121103 (2010).

[8] M. Capizzi and A. Frova, Phys. Rev. Lett. **25**, 1298 (1970).

[9] M. I. Cohen and R. F. Blunt, Phys. Rev. **168**, 929 (1968).

[10] R. U. E.'t Lam, L. G. J. de Haart, A. W. Wiersma, G. Blasse, A. H. A. Tinnemans, and A. Mackor, Mater. Res. Bull. **16**, 1593 (1981).

[11] M. Matsumura, M. Hiramoto, and H. Tsubomura, J. Electrochem. Soc. **130**, 326 (1983).

[12] H. P. Maruska and A. K. Ghosh, Solar Energy Materials **1**, 237 (1979).

[13] A. Monnier and J. Augustynski, J. Electrochem. Soc. **127**, 1576 (1980).

[14] A. Mackor and G. Blasse, Chem. Phys. Lett. **77**, 6 (1981).

[15] G. Blasse, P. H. M. de Korte, and A. Mackor, J. Inorg. Nucl. Chem. **43**, 1499 (1981).

[16] H. Kato and A. Kudo, J. Phys. Chem. B **106**, 5029 (2002).

[17] S. Ouyang, H. Tong, N. Umezawa, J. Cao, P. Li, Y. Bi, Y. Zhang, and J. Ye, J. Am. Chem. Soc. **134**, 1974 (2012).

[18] D. Wang, J. Ye, T. Kako, and T. Kimura, J. Phys. Chem. B **110**, 15824 (2006).

[19] P. Reunchan, S. Ouyang, N. Umezawa, H. Xu, Y. Zhang, and J. Ye, J. Mater. Chem. A **1**, 4221 (2013).

[20] E. Borgarello, J. Kiwi, M. Graetzel, E. Pelizzetti, and M. Visca, J. Am. Chem. Soc. **104**, 2996 (1982).

[21] H. Yasunaga, J. Phys. Soc. Jpn. **24**, 1035 (1968).

[22] Y. Kozuka, Y. Hikita, T. Susaki, and H. Y. Hwang, Phys. Rev. B **76**, 085129 (2007).

[23] T. Feng, Phys. Rev. B **25**, 627 (1982).

[24] G. Li, X. Kuang, S. Tian, F. Liao, X. Jing, Y. Uesu, and K. Kohn, J. Solid State Chem. **165**, 381 (2002).

[25] R. H. Mitchell and A. R. Chakhmouradian, J. Solid State Chem. **144**, 81 (1999).

[26] B. J. Kennedy, C. J. Howard, G. J. Thorogood, M. A. T. Mestre, and J. R. Hester, J. Solid State Chem. **155**, 455 (2000).

[27] E. Assmann, P. Blaha, R. Laskowski, K. Held, S. Okamoto, and G. Sangiovanni, Phys. Rev. Lett. **110**, 078701 (2013).

[28] A. V. Krukau, O. A. Vydrov, A. F. Izmaylov, and G. E. Scuseria, J. Chem. Phys. **125**, 224106 (2006).

[29] J. P. Perdew, K. Burke, and M. Ernzerhof, Phys. Rev. Lett. **77**, 3865 (1996).

[30] F. El-Mellouhi, E. N. Brothers, M. J. Lucero, and G. E. Scuseria, Phys. Rev. B **84**, 115122 (2011).

[31] J. He and C. Franchini, Phys. Rev. B **86**, 235117 (2012).

[32] P. E. Blöchl, Phys. Rev. B **50**, 17953 (1994).

[33] G. Kresse and J. Furthmüller, Phys. Rev. B **54**, 11169 (1996).

[34] H. Iwakura, H. Einaga, and Y. Teraoka, Inorg. Chem. **49**, 11362 (2010).

[35] M. Guennou, P. Bouvier, J. Kreisel, and D. Machon, Phys. Rev. B **81**, 054115 (2010).

[36] K. Oikawa, T. Kamiyama, T. Hashimoto, Y. Shimojyo, and Y. Morii, J. Solid State Chem. **154**, 524 (2000).

[37] A. H. Kahn and A. J. Leyendecker, Phys. Rev. **135**, A1321 (1964).

[38] T. Wolfram, E. A. Kraut, and F. J. Morin, Phys. Rev. B **7**, 1677 (1973).

[39] T. Wolfram, Phys. Rev. Lett. **29**, 1383 (1972).

[40] M. Imada, A. Fujimori, and Y. Tokura, Rev. Mod. Phys. **70**, 1039 (1998).

[41] H. Y. Hwang, Y. Iwasa, M. Kawasaki, B. Keimer, N. Nagaosa, and Y. Tokura, Nat. Mater. **11**, 103 (2012).

[42] H. Chen, A. J. Millis, and C. A. Marianetti, Phys. Rev. Lett. **111**, 116403 (2013).

[43] K. Ueda, H. Tabata, and T. Kawai, J. Appl. Phys. **89**, 2847 (2001).

[44] L. Qiao, T. C. Droubay, M. E. Bowden, V. Shutthanandan, T. C. Kaspar, and S. A. Chambers, Appl. Phys. Lett. **99**, 061904 (2011); K. Yoshimatsu and A. Ohtomo (private communication).

[45] N. Sakai, K. Fukuda, Y. Omomo, Y. Ebina, K. Takada, and T. Sasaki, J. Phys. Chem. C **112**, 5197 (2008).

[46] M. Osada and T. Sasaki, J. Mater. Chem. **19**, 2503 (2009).

[47] N. Ichikawa, Y. Hosaka, T. Saito and Y. Shimakawa, *The 74th Autumn Meeting of the Japan Society of Applied Physics* (JSAP, Tokyo, 2013).